Taylor & Francis
Taylor & Francis Group

RESEARCH ARTICLE

✽ OPEN ACCESS | Check for updates

Guanxin V attenuates myocardial ischaemia reperfusion injury through regulating iron homeostasis

Fuqiong Zhou[a]✽, Zhengguang Zhang[b]✽, Meiyuan Wang[b], Weina Zhu[a], Jie Ruan[a], Hongyan Long[a], Yajie Zhang[a] ⓘ and Ning Gu[c]

[a]Central Laboratory, Nanjing Hospital of Chinese Medicine Affiliated to Nanjing University of Chinese Medicine, Nanjing, China; [b]School of Medicine & Holistic Integrative Medicine, Nanjing University of Chinese Medicine, Nanjing, China; [c]Department of Cardiovascular Disease, Nanjing Hospital of Chinese Medicine Affiliated to Nanjing University of Chinese Medicine, Nanjing, China

ABSTRACT

Context: Guanxin V (GX), a traditional Chinese medicine formula, is safe and effective in the treatment of coronary artery disease. However, its protective effect on myocardial ischaemia reperfusion injury (MIRI) is unclear.

Objective: To investigate the cardioprotective effect of GX on MIRI and explore the potential mechanism.

Materials and methods: Sprague-Dawley male rats were divided into Sham, MIRI and MIRI + GX groups. GX (6 g/kg) was administered to rats via intragastric administration for seven days before ischaemia reperfusion (IR) surgery. The infarct size, histopathology, serum enzyme activities, ultrastructure of the cardiac mitochondria were assessed. H9c2 cells were pre-treated with GX (0.5 mg/mL), and then exposed to hypoxia/reoxygenation (HR). The cell viability and LDH levels were measured. Network pharmacology was conducted to predict the potential mechanism. The related targets of GX were predicted using the TCMSP database, DrugBank database, etc. Finally, pharmacological experiments were used to validate the predicted results.

Results: *In vivo*, GX significantly reduced the myocardial infarct size from 56.33% to 17.18%, decreased the levels of AST (239.32 vs. 369.18 U/L), CK-MB (1324.61 vs. 2066.47 U/L) and LDH (1245.26 vs. 1969.62 U/L), and reduced mitochondrial damage. *In vitro*, GX significantly increased H9c2 cell viability ($IC_{50} = 3.913$ mg/mL) and inhibited the release of LDH (207.35 vs. 314.33). In addition, GX could maintain iron homeostasis and reduce oxidative stress level by regulating iron metabolism-associated proteins.

Conclusions: GX can attenuate MIRI via regulating iron homeostasis, indicating that GX may act as a potential candidate for the treatment of MIRI.

Introduction

Cardiovascular diseases have become a prominent threat to human life and health today. The latest epidemiological data show that cardiovascular diseases cause approximately 17.9 million deaths annually, and this number is estimated to increase to more than 23.6 million by 2030 (D'Souza 2019). Acute myocardial infarction (AMI), as one of the most common cardiovascular diseases, remains a major cause of global morbidity and mortality worldwide, and imposes immense health and economic burden (Domienik-Karłowicz et al. 2021). Clinically, the most effective treatments to reduce the infarct size and improve the clinical outcome are timely myocardial reperfusion using thrombolytic therapy and percutaneous coronary intervention. However, restoration of blood flow in the infracted coronary artery may also induce further cardiomyocyte death and trigger myocardial ischaemia reperfusion injury (MIRI) (Ibanez et al. 2015). MIRI is the leading cause of poor prognosis of AMI and causes multiple cardiac complications. Currently, there remains no effective clinical therapy for preventing myocardial

reperfusion injury. Therefore, new approaches to reduce MIRI are urgently required.

Iron is an indispensable trace metal element in wide range of biological processes, including oxygen transfer, cellular respiration, DNA synthesis, lipid peroxidation, overall metabolism and programmed cell death (Hirst 2013; Abbaspour et al. 2014; Vela 2020). However, iron metabolism imbalance, especially iron overload, exerts potentially deleterious effects due to its involvement in reactive oxygen species (ROS) production (Nakamura et al. 2019). Emerging evidence have demonstrated that iron deposition in cardiac cells, resulting to oxidative stress, participates in the pathophysiological process of MIRI (Ravingerova et al. 2020). Due to the accumulation of excess intracellular iron and iron-dependent overproduction of free radicals in the occurrence, a growing number of clinical studies have suggested that the level of cardiomyocyte iron is an important prognostic factor of MIRI (Paterek et al. 2019; Li et al. 2021). Iron metabolism in MIRI associated diseases involves several mediators, such as hypoxia-inducible factor 1 α (HIF-1α), ferritin heavy chain (FTH) and ferroportin (FPN) (Li et al. 2021). HIF-1α can regulate the transcription of genes involved in iron utilization. HIF-1α,

CONTACT Yajie Zhang ✉ zhangyajie@njucm.edu.cn; Ning Gu ✉ gunning@njucm.edu.cn
✽These authors contributed equally to this work.

presents with visible hyperactivation during MIRI, can enhance transferrin receptor 1 (TFR1) expression and exasperate iron overload, and then ultimately aggravates ROS-induced peroxidative damage (Lok and Ponka 1999; Duarte et al. 2021). In addition, HIF-1α also can regulate ceruloplasmin, which can catalyse the oxidation of ferrous iron (Fe^{2+}) to ferric iron (Fe^{3+}) (Mukhopadhyay et al. 2000), haem oxygenase 1 (HMOX1), which is involved in iron recycling in erythrophagocytosis (Dunn et al. 2021) and divalent metal transporter 1 (DMT1), a protein that promotes iron indraft and inputs iron (Qian et al. 2011). FTH, a major intracellular in storage protein, downregulated in the mouse model of MIRI, resulted in oxidative stress and cardiomyocytes death (Omiya et al. 2009). FPN, the only known cellular iron efflux pump, has also been reported to play a critical role in systemic iron homeostasis (Lakhal-Littleton 2019; Paterek et al. 2019).

At present, as the pathogenesis of cardiovascular diseases (CVD) is rather multifactorial than a single cause, traditional Chinese medicine (TCM) is attracting wide attention in the prevention and treatment of CVD due to its attributes of multicomponent, multi-target and multi-path regulation of the body, and fewer side effects.

According to the theory of traditional Chinese medicine, the pathogenesis of MIRI was mainly due to Qi and Yin deficiency and blood stasis (Du and Zhang 2022). Guanxin V (GX) is a traditional Chinese medicine formula modified from a well-known TCM complex prescription named Shengmai San, which has been clinically utilized for the treatment of ischaemic heart disease. GX consists of *Codonopsis pilosula* (Franch.) Nannf. (Campanulaceae) (Chinese name Dang-Shen), *Ophiopogon japonicas* (L. f) Ker-Gawl. (Liliaceae) (Chinese name Mai-Dong), *Schisandra chinensis* (Turcz.) Baill. (Magnoliaceae) (Chinese name Wu-Wei-Zi), *Salvia miltiorrhiza* Bge. (Lamiaceae) (Chinese name Dan-Shen), *Paeonia lactiflora* Pall. (Ranunculaceae) (Chinese name Chi-Shao) and *Rehmannia glutinosa* Libosch. (Scrophulariaceae) (Chinese name Di-Huang). Among these six TCMs included in GX, Dang-Shen, Mai-Dong and Wu-Wei-Zi are good at enriching Qi, nourishing Yin and promoting the generation of body fluid, Dan-Shen, Chi-Shao and Di-Huang can activate blood, dissipating blood stasis and promote the generation of body fluid (Zuo et al. 2015). Therefore, GX can be used to tonify Qi, nourish Yin and promote blood circulation, which implies its huge potential in MIRI treatment. Actually, GX has been approved to be used in Nanjing Hospital of Chinese Medicine Affiliated to Nanjing University of Chinese Medicine since 2004, and its efficacy and safety in the treatment of coronary artery disease have been confirmed in our clinical studies (Liang et al. 2020). Moreover, our previous studies found that GX could obviously improve the cardiac function, limit infarct size, suppress the inflammatory response and protect against ventricular remodelling in AMI animal models (Liang et al. 2020, 2021, 2022; Zhang et al. 2021). Consistent with AMI, multiple factors, including oxidative stress, systemic inflammation, calcium metabolic disorders, mitochondrial damage and iron overload, have also been demonstrated to be implicated in the pathogenesis and development of MIRI (Bugger and Pfeil 2020; Mahtta et al. 2020; Ramachandra et al. 2020; Vela 2020; Li et al. 2021). Pharmacological studies showed that the TCMs and their components included in GX have the definite protection effects on MIRI. For example, ruscogenin and schisandrin, the main ingredients of Mai-Dong and Wu-Wei-Zi, respectively, exhibit the prominent cardioprotective effects against MIRI through modulating energy metabolism, suppressing inflammation and

oxidative stress (Yang et al. 2021). Dan-Shen and its main components have protective effects against MIRI mainly through ameliorating oxidative stress, inhibiting apoptosis and alleviating inflammation (Song et al. 2013; Huang et al. 2016; Wei et al. 2016; Zeng et al. 2021). Paeonol and paeoniflorin, the main active principles of Chi-Shao, can significantly reduce the myocardial infarct size and reperfusion arrhythmias by activation of the Akt and ERK 1/2 arm of RISK pathway in MIRI rats (Wu et al. 2020; Ma et al. 2022). Catalpol, a kind of iridoid glucoside derived from the roots of Di-Huang, can significantly suppress the process of MIRI and protect oxygen-glucose deprivation/reoxygenation-treated cardiomyocytes through modulating Nrf2/HO-1 signalling axis (Ge et al. 2022). All these findings suggested an extensive clinical value of GX in the treatment of MIRI, which has not been investigated elsewhere.

In this study, the protective effect of GX on MIRI was evaluated, and the potential engaged mechanism predicted via network pharmacology analysis was examined *in vivo* and *in vitro*.

Materials and methods

Reagents

Danshensu, paeoniflorin, rosmarinic acid, salvianolic acid B, salvianic acid A and paeonol (purity > 98%) were all purchased from National Institute for Food and Drug Control (Beijing, China). The kits for determination of aspartate aminotransferase (AST), Creatine kinase-MB (CK-MB), lactate dehydrogenase (LDH), superoxide dismutase (SOD) and malondialdehyde (MDA) were purchased from Nanjing Jiancheng Bioengineering Institute (Nanjing, China). 2,3,5-triphenyltetrazolium chloride (TTC) was purchased from Sigma-Aldrich (St. Louis, MO, USA). AnaeroPack was obtained from MGC (Japan). Dulbecco's modified Eagle medium (DMEM) was obtained from GIBCO (Life Technologies, CA, USA). Foetal bovine serum (FBS) was from AusgeneX (Australia). The serum-free, glucose-free and sodium pyruvate-free DMEM was acquired from Solarbio (Beijing, China). H_2DCFDA kit was obtained from MedChemExpress (Shanghai, China). Iron assay kit, antibody against HIF-1α and FTH were acquired from Abcam (Cambridge, MA, USA). Antibody against FPN was purchased from Novus Biologicals (Littleton, CO, USA). The cell counting kit-8 (CCK-8) and FerroOrange were obtained from Dojindo (Kumamoto, Japan).

The preparation of GX

Codonopsis pilosula, *Ophiopogon japonicas*, *Schisandra chinensis*, *Salvia miltiorrhiza*, *Paeonia lactiflora* and *Rehmannia glutinosa* (the ratio of weight is 20:10:5:20:20:4) were obtained from and deposited at the Department of Pharmacy, Nanjing Hospital of Chinese Medicine Affiliated to Nanjing University of Chinese Medicine. All these herbal medicines were identified by Li Wen, a Chief Pharmacist of Chinese medicine. According to the preparation procedure provided by the Department of Pharmacy, Nanjing Hospital of Chinese Medicine Affiliated to Nanjing University of Chinese Medicine, all of the herbs were soaked in 8 L water for 30 min and then decocted for 90 min. Subsequently, the filter residues were decocted in 6 L of water for 60 min and filtered. The combined aqueous extract was concentrated and further freeze-dried to obtain the powdery extract with a yield of 25.3%.

Animals and treatments

Male adult Sprague-Dawley rats (body weight 200 ± 20 g) were purchased from Shanghai Slaccas Experimental Animal Ltd (Shanghai, China). The animals were housed in environmentally controlled room temperature ($22 \pm 2\,^{\circ}$C) and humidity ($65\% \pm 5\%$) with standard rodent chow and water and 12-h on/off light cycle for a week. All procedures of animal experiments followed the guidelines of the Institutional Animal Ethical Committee of Nanjing University of Chinese Medicine and were approved by the Institutional Animal Care and Use Committee of Nanjing University of Chinese Medicine (Ethical number: 202005A127).

The rats were randomly divided into three experimental groups as follows ($n = 12$, each group): (i) Sham group (normal saline: 10 mL/kg/d), (ii) MIRI group (MIRI + normal saline: 10 mL/kg/d), (iii) MIRI + GX group (GX: 6 g/kg/d). Normal saline and GX were administered to rats via intragastric administration for seven consecutive days before IR surgery. The dosage of GX was converted according to the clinical equivalent dose and the exact dosage of GX on animals was applied according to our previous study (Zhang et al. 2021; Liang et al. 2022a, 2022b).

The rat MIRI model was established by left anterior descending coronary artery ligation. Briefly, after anaesthesia, the rats were fixed and plugged into a small animal ventilator. Then the intercostal space between third and fourth rib of the left chest was exposed, and the heart was exposed entirely after tearing the pericardium. Subsequently, the left anterior descending coronary artery was ligated with a 6–0 silk suture at approximately 2 mm below the left atrial appendage. The electrocardiogram was utilized to monitor the ST-segment elevation. After 30 min of ischaemia, the ligature loosened and followed by 2 h of reperfusion. For the Sham group, the rats were subjected to the same surgical procedures without ligating the left anterior descending coronary artery. At the end of the reperfusion, the blood samples were collected from abdominal aorta of experimented rats to separate out serum by centrifugation at 3000 rpm for 10 min at $4\,^{\circ}$C. Finally, after euthanized with an overdose of pentobarbital (200 mg/kg, i.p.), the hearts of the rats were harvested for further analysis.

Measurement of myocardial infarct size

The hearts of rats were flushed with saline and frozen in $-20\,^{\circ}$C for 30 min. Then the ventricles were sliced into 5 mm sections and incubated in 1% TTC solution at $37\,^{\circ}$C for 15 min in the dark. After being washed three-times, these sections were photographed, the myocardial infarction area was white and non-infarction area was red. The infarct size was analysed and calculated by Image J.

Masson's trichrome staining

After the experiment, the myocardial tissues were harvested and fixed into 4% paraformaldehyde. The samples were dehydrated in a graded series of ethanol (50, 75, 85, 95 and 100%), and then paraffin-embedded and cut into 4 μm thick sections. The sections were dewaxed with xylene and soaked in an alcohol gradient. Then sections were incubated with different solutions supplemented in Masson's Trichrome Stain Kit (Solarbio G1345). Finally, the sections were treated with the 1% acetic acid solution, dehydrated, mounted with mounting solution and observed using light microscopy (Olympus CKX41, Japan).

Measurement of biological parameters in the serum

The AST, CK-MB and LDH levels in the serum were measured using commercial ELISA kits (Nanjing Jiancheng Bioengineering Institute) following the manufacturer's protocols exactly.

Ultrastructural analysis by transmission electron microscope (TEM)

The heart tissues were fixed with 2.5% glutaraldehyde and cut into ultra-thin sections. After being fixed with 1% osmic acid for 1 h, the sections were dehydrated in a graded alcohol series and embedded. Subsequently, these sections were sliced and stained with uranyl acetate and lead citrate. The ultrastructure images of the cardiac mitochondria were observed and imaged under transmission electron microscope (Hitachi, Tokyo, Japan).

Cell culture and HR injury model in vitro

Rat H9c2 cardiomyocyte cell line was purchased from Shanghai Institute of Cell Biology, Chinese Academy of Sciences (Shanghai, China). The cells were cultured with the supplemented DMEM solution containing 10% foetal bovine serum and double antibiotics (penicillin and streptomycin, 100 μg/mL:100 μg/mL) at $37\,^{\circ}$C in a humidified atmosphere of 5% CO_2. To establish the HR model, the cells were washed twice with PBS and cultured with the glucose-free DMEM base medium in an AnaeroPack System, in which oxygen was deprived (Wei et al. 2018; Li et al. 2019; Zhang et al. 2020; Wen et al. 2021). After 3 h, the plate was taken out and cultured with normal culture medium in a normoxic incubator at $37\,^{\circ}$C for 2 h to mediate reoxygenation. The following groups were tested: (1) Control group: the cells were cultured under normal conditions; (2) GX group: the cells were pre-treated with GX for 12 h before and during maintenance under normal conditions; (3) HR group: the cells were exposed to hypoxia for 3 h and reoxygenation for 2 h; (4) HR + GX group: the cells were pre-treated with GX for 12 h prior to and during HR treatment.

Cell viability assays

After cells were cultured and treated in 96-well plates, 10 μL of CCK-8 reagent (Dojindo, Japan) was added to each well and then incubated for 1 h in the dark. Absorbance was measured at 450 nm using a multifunction microplate reader (Bio-Tek, Winooski, VT, USA). The assays were repeated three times.

Measurement of LDH release in H9c2 cells

Cell supernatant was collected to measure LDH level using the LDH assay kit (Nanjing Jiancheng Bioengineering Institute). Using a microplate reader (490 nm wavelength), the absorbance was determined.

Network pharmacology analysis

Targets collection

The active targets of GX were obtained from the traditional Chinese medicine systems pharmacology (TCMSP) database and encyclopaedia of traditional Chinese medicine (ETCM) database. The effective compounds were screened using oral bioavailability (OB) $\geq 30\%$ and drug-likeness (DL) ≥ 0.18.

The targets of MIRI were selected using GeneCards, OMIM, DrugBank, TTD databases. All sets of data were combined and the duplicates were removed.

A Venn diagram was drawn via Omicshare Tools (https://www.omicshare.com) to show overlapping targets between the predicted targets of GX and the disease targets of MIRI.

Network construction and analysis

The active ingredients of GX and the overlapping targets were input into Cytoscape 3.8.0 software to construct and visualize the compound-target network. Then the overlapping targets were further analysed by STRING database to establish a protein–protein interaction (PPI) network. Finally, Gene Ontology (GO) function analysis and Kyoto Encyclopaedia of Genes and Genomes (KEGG) pathway enrichment analysis of overlapping targets were performed using DAVID, and the results were visualized by Omicshare Tools.

Measurement of the cardiac MDA and SOD

The cardiac MDA level and SOD activity were measured using a kit (Nanjing Jiancheng Bioengineering Institute) in accordance with the manufacturer's instructions.

Measurement of intracellular ROS production

The intracellular ROS generation was assessed using H_2DCFDA kit according to the manufacturer's instructions. Then the cells were washed twice with PBS and the DCF fluorescence intensity was observed under a fluorescence microscope (Olympus BX63, Japan). Image J software was used to analyse the data.

Moreover, trypsin-digested cells were washed with PBS and stained with probe, then analysed by a flow cytometer (Cytomics^{TM} FC 500, Beckman Coulter, CA, USA) and FlowJo software.

Prussian blue staining

To confirm the free iron in heart tissue sections, a Prussian blue stain kit was carried out according to the manufacturer's instructions. The heart slices were dewaxed and dehydrated, and then incubated with Prussian blue and washed by PBS. Finally, a light microscope was used to observe the stained sections.

Iron assay

Total iron contents of tissues and cells were quantified using an iron assay kit (Abcam, ab83366). In short, samples were collected, washed with cold PBS, homogenized in iron assay buffer and homogenized in iron assay buffer, Next, iron-reducing agent was added to the samples for total iron (Fe^{3+} and Fe^{2+}) analysis. Finally, the iron probe solution was added for incubation at $25 \,^{\circ}C$ in dark conditions for 1 h. The content was immediately measured using the multifunction microplate reader under the wavelength of 593 nm.

Intracellular iron assay

The intracellular iron concentration was assessed using FerroOrange probe. Cells were seeded in 6-well plates and treated with the indicated treatment. FerroOrange (1 μM)

dispersed in serum-free medium was added to the cells, and the cells were incubated for 30 min at $37 \,^{\circ}C$. Then the fluorescence intensity was observed under a fluorescence microscope.

Immunohistochemical detection

The myocardial sections were immersed with 3% methanol-H_2O_2 for 10 min and incubated with primary antibodies (1:1000) against HIF1α, FPN and FTH for immunostaining at room temperature for 2 h and an appropriate anti-mouse secondary antibody for 1 h. Immunostaining was performed by 3,3′-diaminobenzidine solution for 5 min at room temperature. The samples were visualized under a light microscope.

Western blot analysis

H9c2 cells were lysed with RIPA lysis buffer before determining the protein concentrations using a BCA kit (Beyotime, Shanghai, China). Isolated protein (30 μg) was separated by 10% SDS-PAGE gels, then transferred onto polyvinylidene fluoride membranes (PVDF, Millipore, USA). After blocking with non-fat milk solution (5%) for 1 h, primary antibodies were incubated with the membranes overnight at $4 \,^{\circ}C$. After washing, the samples were incubated with secondary antibodies for 1 h at room temperature. Finally, the protein bands were visualized with enhanced chemiluminescence.

Statistical analysis

All data are expressed as mean ± standard deviation (SD). All statistical analyses were performed using GraphPad Prism 8.0 software. Statistical differences were accessed by one-way analysis of variance (ANOVA), and $p < 0.05$ was considered statistically significant.

Results

GX treatment attenuated myocardial ischaemia-reperfusion injury and HR-induced H9c2 cardiomyocytes damage

We first investigated whether GX could protect cardiomyocytes against MIRI *in vivo*. As shown in Figure 1(A), GX significantly reduced the infarct size in rats subjected to MIRI. The ST segment of the MIRI group was observably elevated, but when GX pre-treatment, this change was reversed (Figure 1(B)). Besides, the Masson's trichrome staining showed that the myocardial fibrosis degree in the MIRI group was higher than that in the Sham group, whereas GX treatment attenuated MIRI-induced cardiac fibrosis (Figure 1(C)). Furthermore, the myocardial enzymes in the serum such as AST, CK-MB and LDH were measured to assess myocardial injury (Figure 1(D)). The activities of AST, CK-MB and LDH enzymes increased remarkably in the MIRI group, indicating that a serious damage may occur in the heart. Interestingly, these increases of myocardial enzymes were significantly attenuated after GX treatment. Compared with the Sham group, the myocardial mitochondria of the MIRI group were severely distorted, the outer mitochondrial membranes were ruptured, the cristae were vague, melted and even vacuolization. However, GX treatment significantly reduced the mitochondrial damage compared with those of the MIRI group (Figure 1(E)).
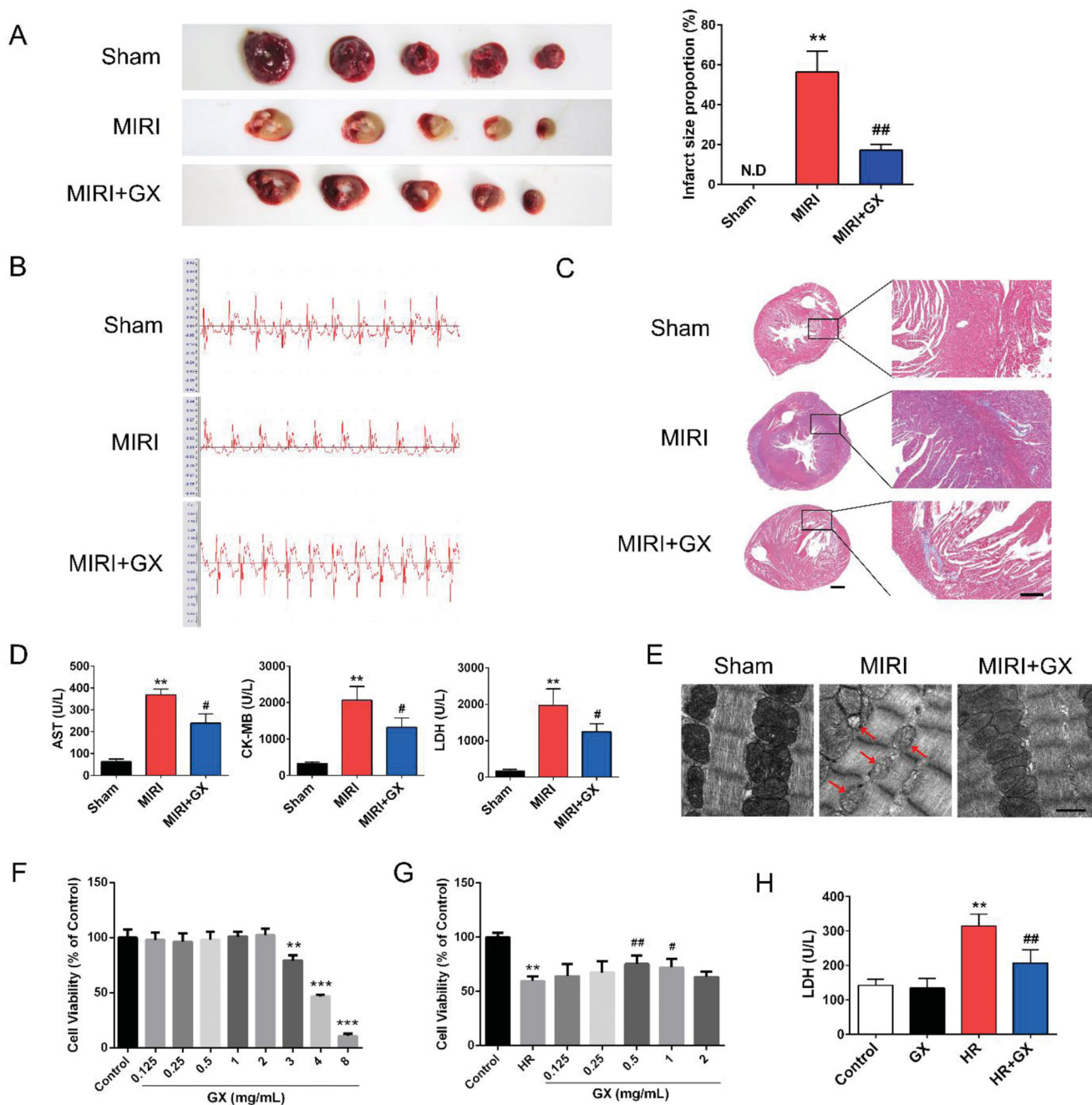
Figure 1. GX treatment attenuated myocardial ischaemia-reperfusion injury and HR-induced H9c2 cardiomyocytes damage. (A) Representative images of heart sections stained by TTC. $n = 4$. N.D, no detectable. (B) The electrocardiographs of each group. (C) Representative images of Masson's trichrome staining in heart tissue. Scale bar, 2 mm (left) and 500 μm (right). (D) The levels of AST, CK-MB and LDH in the serum. $n = 6$. (E) The representative TEM images of heart tissues. Scale bar, 1 μm, $n = 3$. (F) Cell viability of H9c2 cells pre-treated with various concentrations of GX for 24 h. $n = 6$. (G) Effects of GX on HR-induced H9c2 cells. $n = 6$. (H) The release of LDH in the supernatant of HR-induced H9C2 cells. $n = 6$. Data were expressed as the means ± SD analysed by one-way ANOVA. $*p < 0.05$, $**p < 0.01$ vs. Sham or Control; $^{\#}p < 0.05$, $^{\#\#}p < 0.01$ vs. MIRI or HR.

To further explore the protective effects of GX on cardiomyocytes, we established the HR (4-h hypoxia followed by 4-h reoxygenation) model in H9c2 cells. According to Figure 1(F), the increase concentration of GX from 0.125 to 2 mg/mL for 24 h did not cause apparent cytotoxicity in H9c2 cells under normal conditions. The calculated IC_{50} value was 3.913 mg/mL. As shown in the Figure 1(G), the cell viability of the HR group decreased remarkably compared with the control group, whereas GX treatment increased the cell viability after HR injury in a dose-dependent manner. At the concentration of 0.5 mg/mL, GX provided maximal protection on cardiomyocytes, so 0.5 mg/mL

GX was selected to conduct the following experiments. The release of LDH was significantly increased in the HR-induced H9c2 cells, whereas 0.5 mg/mL GX alleviated the increased LDH release (Figure 1(H)). All these findings indicated that GX had an excellent protective effect on MIRI.

Network pharmacology analysis

After integrating information from TCMSP and ETCM databases, a total of 100 active compounds in GX and 213

Table 1. Ninety-one overlapping targets between GX and MIRI.

No.	Gene names	Protein names
1	ACHE	Acetylcholinesterase
2	ADRA1A	Alpha-1A adrenergic receptor
3	ADRA1B	Alpha-1B adrenergic receptor
4	ADRA1D	Alpha-1D adrenergic receptor
5	ADRA2A	Alpha-2A adrenergic receptor
6	ADRA2B	Alpha-2B adrenergic receptor
7	ADRA2C	Alpha-2C adrenergic receptor
8	ADRB1	Beta-1 adrenergic receptor
9	ADRB2	Beta-2 adrenergic receptor
10	AHR	Aryl hydrocarbon receptor
11	AKR1C3	Aldo-keto reductase family 1 member C3
12	AKT1	Threonine-protein kinase
13	APP	Amyloid beta A4 protein
14	AR	Androgen receptor
15	BCL2	Apoptosis regulator Bcl-2
16	CALM1	Calmodulin
17	CASP3	Caspase-3
18	CCND1	G1/S-specific cyclin-D1
19	CHRM1	Muscarinic acetylcholine receptor M1
20	CHRM2	Muscarinic acetylcholine receptor M2
21	CHRM3	Muscarinic acetylcholine receptor M3
22	CHRM4	Muscarinic acetylcholine receptor M4
23	CHRM5	Muscarinic acetylcholine receptor M5
24	CHRNA2	Neuronal acetylcholine receptor subunit alpha-2
25	CHRNA7	Neuronal acetylcholine receptor subunit alpha-7
26	DPP4	Dipeptidyl peptidase IV
27	DRD1	Dopamine D1 receptor
28	DRD2	Dopamine D2 receptor
29	DRD5	Dopamine D5 receptor
30	EDNRA	Endothelin-1 receptor
31	EGFR	Epidermal growth factor receptor
32	ESR1	Estrogen receptor
33	ESR2	Estrogen receptor beta
34	F10	Coagulation factor Xa
35	F2	Kinetochore protein Nuf2
36	F7	Coagulation factor VII
37	FOS	Proto-oncogene c-Fos
38	GABRA1	Gamma-aminobutyric acid receptor subunit alpha-1
39	GABRA2	Gamma-aminobutyric acid receptor subunit alpha-2
40	GABRA3	Gamma-aminobutyric acid receptor subunit alpha-3
41	GABRA5	Gamma-aminobutyric acid receptor subunit alpha-5
42	GABRA6	Gamma-aminobutyric acid receptor subunit alpha-6
43	GABRE	Gamma-aminobutyric acid receptor subunit epsilon
44	GABRG3	Gamma-aminobutyric acid receptor subunit gamma-3
45	GSK3B	Glycogen synthase kinase-3 beta
46	HIF1A	Hypoxia-inducible factor 1-alpha
47	HTR1A	5-Hydroxytryptamine 1A receptor
48	HTR1B	5-Hydroxytryptamine 1B receptor
49	HTR2A	5-Hydroxytryptamine 2A receptor
50	HTR2C	5-Hydroxytryptamine 2C receptor
51	HTR3A	5-Hydroxytryptamine receptor 3A
52	IL10	Interleukin-10
53	IL6	Interleukin-6
54	ITGB3	Integrin beta-3
55	KCNH2	Potassium voltage-gated channel subfamily H member 2
56	LTA4H	Leukotriene A-4 hydrolase
57	MAOA	Amine oxidase [flavin-containing] A
58	MAOB	Amine oxidase [flavin-containing] B
59	MAPK14	Mitogen-activated protein kinase 14
60	MDM2	E3 ubiquitin-protein ligase Mdm2
61	MIF	Macrophage migration inhibitory factor
62	MMP2	Matrix metalloproteinase-2
63	MMP9	Matrix metalloproteinase-9
64	MYC	Myc proto-oncogene protein
65	NFKBIA	NF-kappa-B inhibitor alpha
66	NOS2	Nitric oxide synthase, inducible
67	NOS3	Nitric oxide synthase, endothelial
68	NR1I2	Nuclear receptor subfamily 1 group I member 2
69	NR1I3	Nuclear receptor subfamily 1 group I member 3
70	NR3C2	Mineralocorticoid receptor
71	OPRM1	Mu-type opioid receptor
72	PCNA	Proliferating cell nuclear antigen
73	PDE3A	CGMP-inhibited 3′,5′-cyclic phosphodiesterase A

(continued)

Table 1. Continued.

No.	Gene names	Protein names
74	PON1	Serum paraoxonase/arylesterase 1
75	PPARG	Peroxisome proliferator activated receptor gamma
76	PRKCA	Protein kinase C alpha type
77	PRKCB	Protein kinase C beta type
78	PTGS1	Prostaglandin G/H synthase 1
79	PTGS2	Prostaglandin G/H synthase 2
80	RXRA	Retinoic acid receptor RXR-alpha
81	SCN5A	Sodium channel protein type 5 subunit alpha
82	SHBG	Sex hormone-binding globulin
83	SLC6A2	Sodium-dependent noradrenaline transporter
84	SLC6A3	Sodium-dependent dopamine transporter
85	SLC6A4	Sodium-dependent serotonin transporter
86	STAT3	Signal transducer and activator of transcription 3
87	TNF	Tumor necrosis factor
88	TOP2A	DNA topoisomerase 2-alpha
89	TOP2B	DNA topoisomerase 2-beta
90	TUBB	Tubulin beta chain
91	VEGFA	Vascular endothelial growth factor A

compound-related targets were acquired. Besides, the 512 MIRI-related targets were searched from GeneCards, OMIM, DrugBank, TTD databases. A Venn diagram was constructed and 91 overlapping targets between GX and MIRI were obtained (Table 1). These overlapping targets were considered as potential targets of GX in the prevention and treatment of MIRI. Next, the 72 compounds and 91 overlapping targets were input into Cytoscape software to build the active compound-target network (Figure 2). The main active compounds of GX (top 20) are shown in Table 2. In the network, the orange rhombuses represented active compounds, and the light blue ovals represented overlapping targets. Then, the above 91 overlapping targets were submitted to the STRING database to construct a PPI network, which involved 91 nodes and 738 edges (Figure 3(A)). Subsequently, the relevant information of PPI network was imported into Cytoscape software to perform topological analysis. After screening according to Degree value $\geq$ 20 (Yong et al. 2021), a total of 31 core targets in the PPI network were extracted (Figure 3(B)). The size and colour of the nodes reflected the values of degree, and the top 15 targets were AKT1, TNF, IL6, EGFR, FOS, VEGFA, ESR1, PTGS2, MYC, CASP3, MMP9, HIFIA, NOS3, PPARG and STAT3.

To further explore functions of the overlapping targets, GO and KEGG pathway enrichment analyses were performed using the DAVID online analysis platform. With P value < 0.05 as the screening criterion, a total of 216 biological process (BP)-related items and 91 KEGG pathways were screened out. The GO enrichment analysis results (Figure 4(A)) and the top 20 KEGG pathways (Figure 4(B)) were visualized by the Omicshare Tools. As shown in Figure 4(A), response to iron ion was the key biological process involved in the prevention and treatment of MIRI with GX. In addition, the KEGG pathways mainly included HIF-1 signalling pathway, Calcium signalling pathway and TNF signalling pathway. These results indicated that GX might play a protective role against MIRI by regulating the above multiple pathways. Studies have reported that HIF-1, a heterodimer consisting of an oxygen-regulated α subunit and a constitutively expressed β subunit, can regulate a series of genes that participate in iron metabolism (Romney et al. 2011; Zhang et al. 2011; Hirota 2019), so we further investigated whether iron metabolism was involved in the protection of GX against MIRI.

Figure 2. Active compound-target network. The orange rhombus nodes represent the molecular identification (MOL ID) number of active components in GX, and the blue oval nodes represent the overlapping targets.

GX treatment improved oxidative stress *in vivo* and *in vitro*

We further investigated the effects of GX on oxidative stress after myocardial ischaemia-reperfusion in rats. As shown in Figure 5(A,B), the activity of SOD was significantly suppressed and the level of MDA dramatically increased after ischaemia reperfusion. Intriguingly, these changes were effectively rescued by GX treatment.

To assess the intracellular ROS levels, the ROS-sensitive probe H_2DCFDA was used. The intracellular ROS production was monitored by fluorescence microscopy and flow cytometry assay. After HR treatment, the DCF fluorescence intensity was significantly increased compared with the control group. Although GX pre-treatment alone showed no effect on ROS production, it remarkably reduced the level of ROS in the HR + GX group (Figure 5(C)). This was accompanied by the results of flow

cytometry assay (Figure 5(D)). To sum up, these results revealed that GX could mitigate HR-induced ROS generation in H9c2 cells.

GX suppressed iron accumulation *in vivo* and *in vitro*

To determine the effect of GX treatment on MIRI-induced iron deposition in rats, Prussian blue staining was applied as shown in Figure 6(A). Little dark blue staining was observed in the Sham group, whereas the distinct iron accumulation in the heart tissue of the MIRI group was displayed. By contrast, GX treatment reduced the number of dark blue staining. Furthermore, the total iron content in the heart tissues was tested with iron assay kit. We found the increased total iron content in the MIRI

Table 2. The main active components of GX in the prevention and treatment of MIRI (top 20).

MOL ID	Compound name	Degree
MOL01	(+)-Catechin	4
MOL02	2′-Hydroxymethylophiopogonone A	2
MOL03	2-Isopropyl-8-methylphenanthrene-3,4-dione	4
MOL04	3-Beta-hydroxymethyllenetanshiquinone	1
MOL05	3α-Hydroxytanshinonella	7
MOL06	4-Methylenemiltirone	22
MOL07	5,6-Dihydroxy-7-iopropyl-1,1-dimethyl-2,3-dihydrophenanthren-4-one	3
MOL08	5,7-Dihydroxy-6,8-dimethyl-3-(4′-hydroxy-3′-methoxybenzyl)Chroman-4-One	6
MOL09	6-Aldehydo-Isoophiopogone B	7
MOL10	7-Methoxy-2-methyl isoflavone	29
MOL11	Adenosine	4
MOL12	Angeloylgomisin O	3
MOL13	Beta-sitosterol	8
MOL14	Camphor	2
MOL15	Caproic Acid	2
MOL16	Cryptotanshinone	16
MOL17	Danshenol A	5
MOL18	Danshenol B	2
MOL19	Danshenspiroketallactone	3
MOL20	Danshenxinkum	15
MOL21	Dehydrotanshinone II A	13
MOL22	Deoxyharringtonine	2
MOL23	Deoxyneocryptotanshinone	5
MOL24	Dihydrotanshinlactone	7
MOL25	Dihydrotanshinonel	6
MOL26	Ellagic acid	7
MOL27	Epidanshenspiroketallactone	2
MOL28	Formyltanshinone	1
MOL29	Frutinone A	11
MOL30	Glycitein	12
MOL31	Gomisin A	2
MOL32	Gomisin G	1
MOL33	Gomisin R	5
MOL34	Isocryptotanshinone	15
MOL35	Isotanshinone II	8
MOL36	Longikaurin A	5
MOL37	Luteolin	19
MOL38	Methyl ophiopogonanone B	5
MOL39	Methyl-3-(3′,4′-dihydroxybenzyl) Chroman-4-One	1
MOL40	Methylenetanshinquinone	8
MOL41	Miltionone I	1
MOL42	Miltirone	11
MOL43	Neocryptotanshinone	4
MOL44	Neocryptotanshinone ii	14
MOL45	Ophiopogon A	3
MOL46	Ophiopogonanone B	2
MOL47	Ophiopogonanone D	6
MOL48	Ophiopogonanone E	1
MOL49	Ophiopogonanone F	1
MOL50	Paeoniflorgenone	2
MOL51	Paeoniflorin	2
MOL52	Perlolyrine	3
MOL53	Poriferasterol	1
MOL54	Prolithospermic acid	4
MOL55	Przewalskin a	1
MOL56	Przewalskin b	1
MOL57	Przewaquinone B	3
MOL58	przewaquinone c	13
MOL59	Przewaquinone E	2
MOL60	przewaquinone f	2
MOL61	Salvianolic acid a	3
MOL62	Salvianolic acid j	1
MOL63	Salvilenone	4
MOL64	Salviolone	26
MOL65	Schizandrer B	2
MOL66	Spinasterol	1
MOL67	Stigmasterol	22
MOL68	Tanshinaldehyde	6
MOL69	Tanshindiol B	2
MOL70	Tanshinone VI	4
MOL71	Tanshinonella	21
MOL72	Wuweizisu C	2

Figure 3. Construction of the PPI network. (A) The PPI network model. (B) The PPI network of core targets extracted from degree centrality.
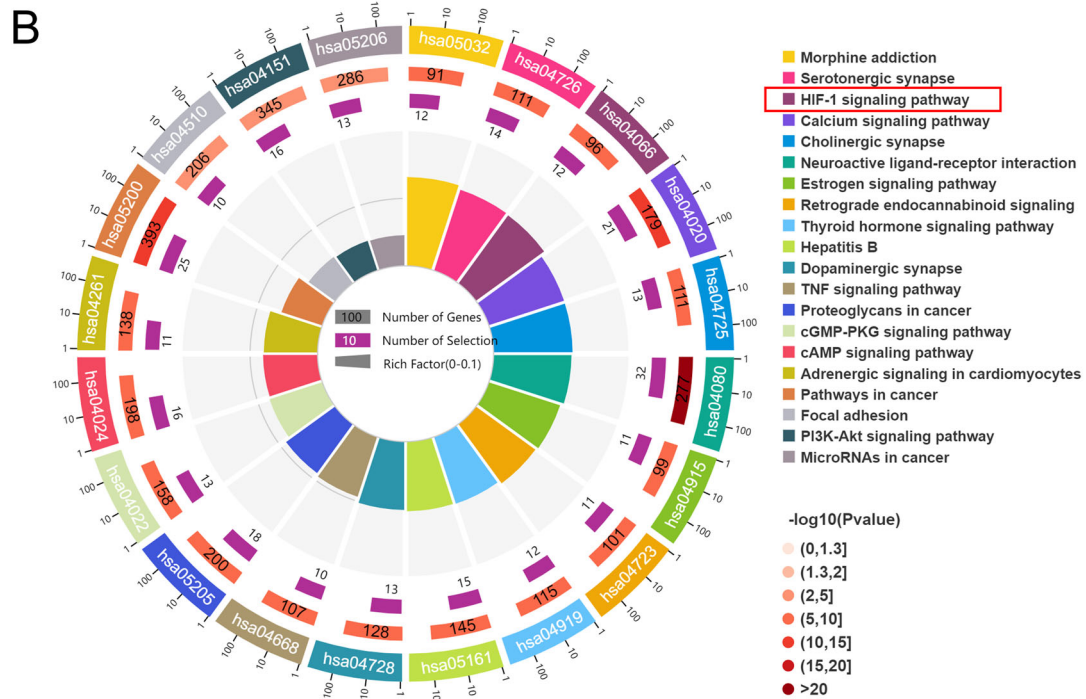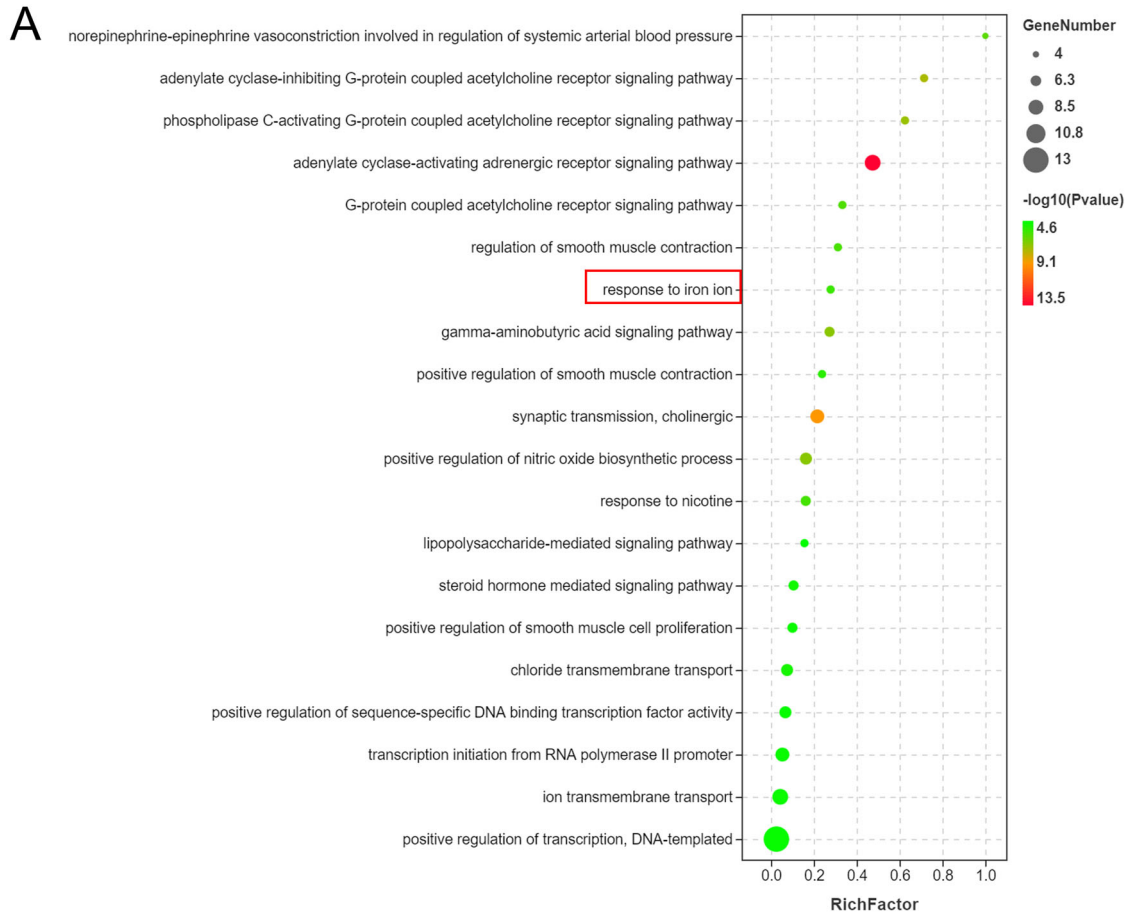
Figure 4. Enrichment analysis of biological process (BP) and KEGG pathway. (A) GO enrichment analysis of BP. The top 20 BPs were selected to draw the bubble diagram. (B) KEGG pathway enrichment analysis. The top 20 KEGG pathways were selected to draw the circle chart.
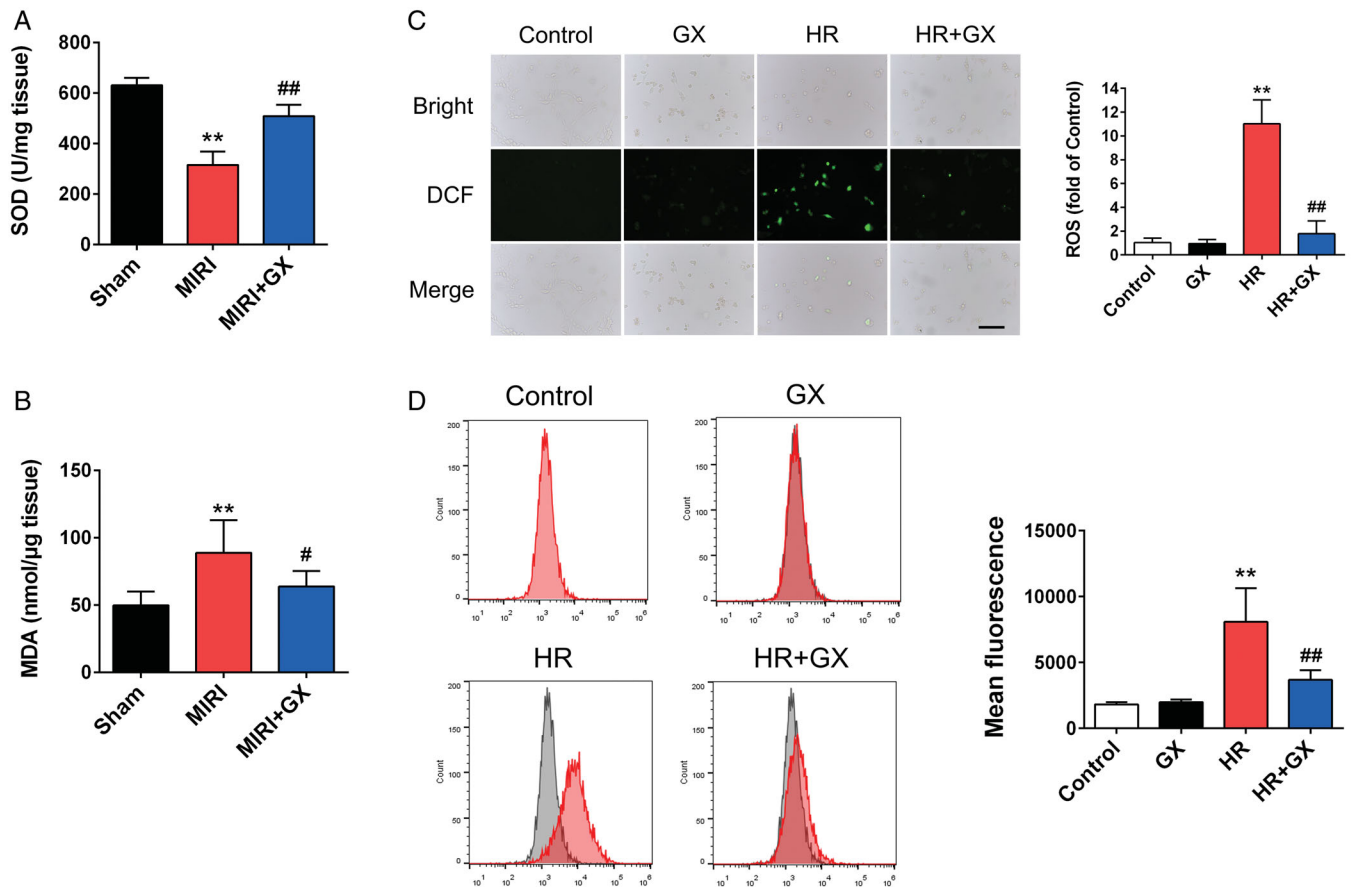
Figure 5. GX treatment improved oxidative stress *in vivo* and *in vitro*. (A) Myocardial MDA and (B) SOD activities. (C) Representative ROS levels of H9c2 cells measured by incubating with the H$_2$DCFDA probe. Scale bar, 100 μm. (D) DCFH fluorescence measured by flow cytometry. Data were expressed as the means ± SD analysed by one-way ANOVA ($n = 3$). $^{**}p < 0.01$ vs. Sham or Control; $^{#}p < 0.05$, $^{##}p < 0.01$ vs. MIRI or HR.

rats, whereas treatment with GX significantly inhibited the iron increase (Figure 6(C)).

Moreover, intracellular iron levels in H9c2 cells were measured using FerroOrange. The cells in the HR group emitted much stronger orange fluorescence compared with the control group. Treatment with GX did not affect iron accumulation in H9c2 cells but decreased the HR-induced increase in the orange fluorescence intensity (Figure 6(B)). The increased iron content was discovered in HR group. However, such an increase in iron content was remarkably eliminated by pretreating the H9c2 cells with 0.5 mg/mL GX (Figure 6(D)). These data demonstrated that GX could ameliorate the iron accumulation both in myocardial tissue and H9c2 cells.

GX inhibited HIF1α, increased FPN and FTH expression in vivo *and* in vitro

The current researches have demonstrated that iron metabolism imbalance, especially iron overload, has been proved to be correlated with the pathology of MIRI, and multiple iron metabolism associated factors are implicated in the pathogenesis of MIRI (Ravingerova et al. 2020; Li et al. 2021). To validate whether the protective mechanism of GX on MIRI are associated with iron metabolism, immunohistochemical staining and Western blot analyses were conducted to examine the role of GX pre-treatment in the expression of HIF1α, FPN and FTH *in vivo* and *in vitro*. As shown in Figure 7(A,B), immunohistochemical staining of the heart tissues revealed a higher level of the expression

of HIF1α and a lower level of the expression of FPN and FTH in the MIRI group compared with that in the Sham group. After pre-treatment with GX reversed the above levels, the expression of HIF1α was decreased and the expression of FPN and FTH was increased effectively. Consistent with *in vivo* experiments, the results of Western blot demonstrated that HR treatment upregulated the protein expression of HIF1α, but also simultaneously downregulated the expression of FPN and FTH in HR injured H9c2 cells. Similarly, GX treatment prevented HR-induced upregulation of HIF1α and downregulation of FPN and FTH (Figure 7(C)). Collectively, our research results revealed that GX could maintain iron homeostasis via regulating iron metabolism-associated factors both *in vivo* and *in vitro*.

Discussion

GX is an in-hospital preparation developed by Professor Ning Gu, a famous TCM physician of Jiangsu, according to his long-term clinical experience. GX has been applied for the clinical treatment of coronary heart disease for nearly 20 years. Meanwhile, our previous animal experiments have shown that GX could trigger ventricular remodelling via significantly improving the cardiac function, the blood flow dynamics and reducing serum levels of inflammatory factors in AMI rats. In this study, we confirmed the cardioprotective effects of GX against MIRI *in vivo* and HR injury *in vitro* via reduction of iron accumulation and oxidative stress. Mechanistically, GX
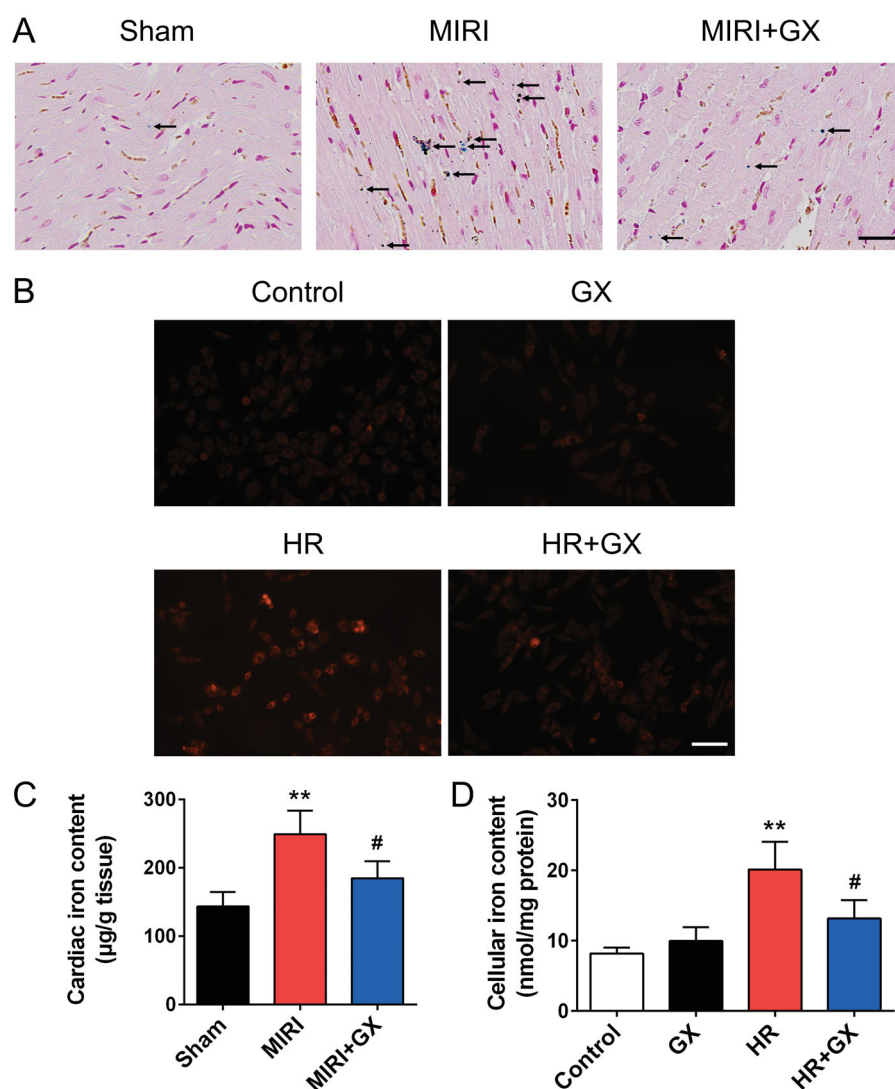
Figure 6. GX suppressed iron accumulation *in vivo* and *in vitro*. (A) Representative images of iron deposition stained by Prussian blue. Scale bar, 50 μm. (B) The intracellular iron levels in H9c2 cells measured by FerroOrange. Scale bar, 100 μm. (C) The total iron contents of the heart tissues detected by iron assay kit. (D) The total iron contents of H9c2 detected by iron assay kit. Data were expressed as the means ± SD analysed by one-way ANOVA ($n = 3$). **$p < 0.01$ vs. Sham or Control; #$p < 0.05$ vs. MIRI or HR.

could regulate iron metabolism-related proteins to maintain heart iron homeostasis.

The multi-components and multi-targets of TCM formula make it difficult to elucidate the underlying therapeutic mechanisms. Recently, network pharmacology is widely used to predict the bioactive ingredients of TCM and clarify the mechanism across multiple components, targets and pathways (Cui et al. 2021). Here, we integrated network pharmacology prediction and experimental validation to explore the potential engaged mechanism of GX in alleviating MIRI. In our present study, a total of 100 active ingredients in GX and 213 compound-related targets were acquired from TCMSP and ETCM databases. Then we searched 512 MIRI-related targets from GeneCards, OMIM, DrugBank and TTD databases. Next, 91 overlapping targets between GX and MIRI were obtained via constructing a Venn diagram. The GO function analysis showed that the above 91 overlapping targets were enriched for various biological processes, and response to iron ion was the crucial biological process involved in GX-provided protection against MIRI. Furthermore, KEGG pathway analysis found that GX could affect multiple pathways, including HIF-1 signalling pathway, Calcium signalling

pathway and TNF signalling pathway. There is increasing evidence that iron metabolic imbalances participate in the pathophysiological process of MIRI. Furthermore, a recent clinical study using cardiac magnetic resonance imaging showed that the presence of myocardial haemorrhage was followed by the residual myocardial iron in post-MI patients received reperfusion therapy (Bulluck et al. 2016). Iron homeostasis is achieved through the coordination of various iron metabolism-related proteins, and HIF-1 is a pivotal regulator of iron metabolism in MIRI. Taken together, the results of network pharmacology indicated that GX could attenuate MIRI by regulating iron metabolic balance and maintaining iron homeostasis. Next, we further validated these prediction results from network pharmacology in the next following experiments.

When ischaemia-reperfusion occurs, mitochondrial damage can induce ROS production. Oxidative stress triggered by excessive ROS is one of the most important initiators for MIRI, which can cause irreversible cardiomyocyte damage and cardiac dysfunction (Xiang et al. 2021). Moreover, uncontrolled accumulation of iron can induce oxidative stress, catalyse the redundant oxygen-free radicals and overproduction of ROS via the Fenton
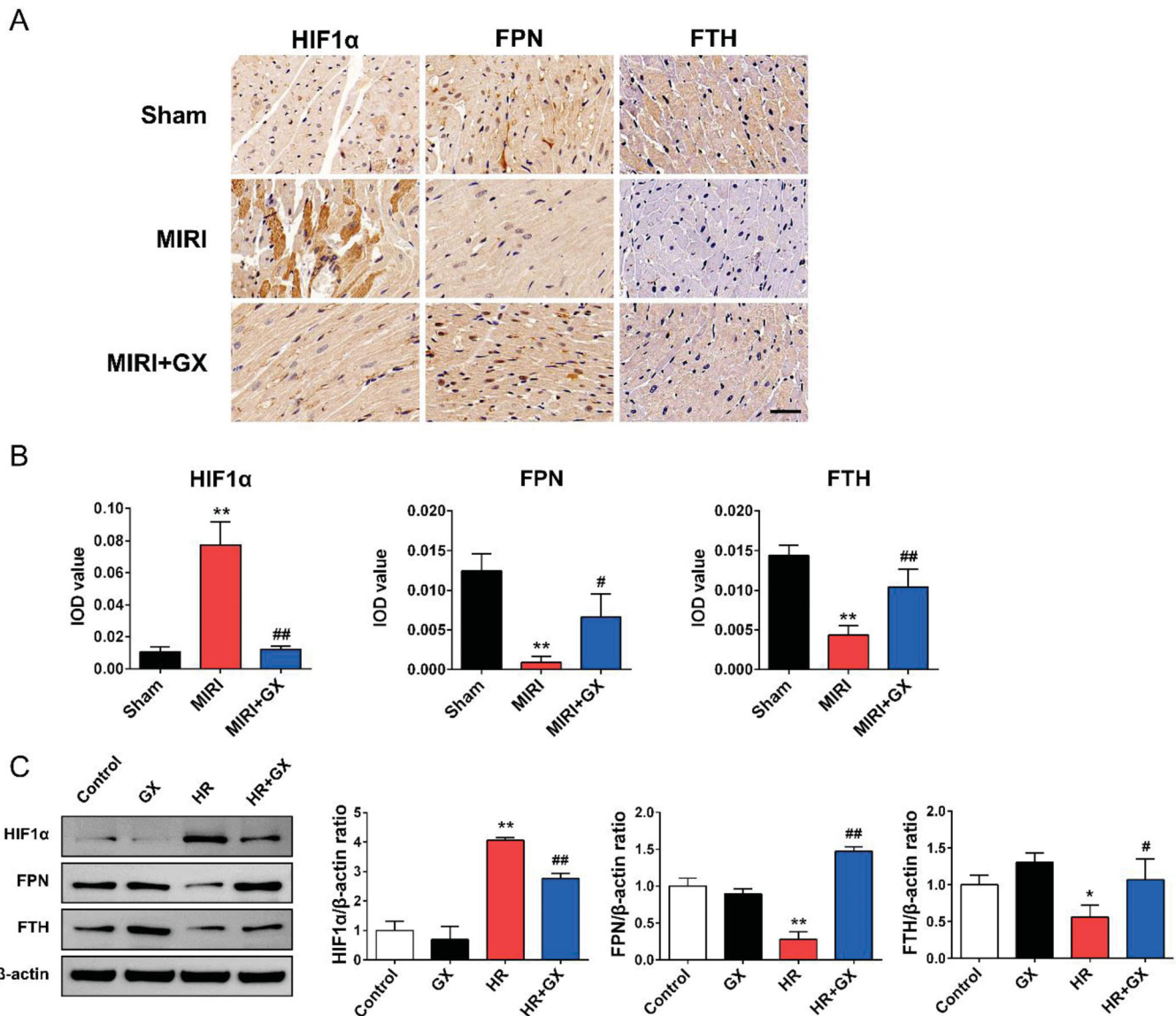
Figure 7. GX inhibited HIF1α, increased FPN and FTH expression *in vivo* and *in vitro*. (A,B) The expression of HIF1α, FPN and FTH detected by immunohistochemical staining in heart tissues. Scale bar, 50 μm. (C) The protein levels of HIF1α, FPN and FTH measured by Western blot in H9c2 cells. Data were expressed as the means ± SD analysed by one-way ANOVA (*n* = 3). *$p < 0.05$, **$p < 0.01$ vs. Sham or Control; #$p < 0.05$, ##$p < 0.01$ vs. MIRI or HR.

reaction and Haber-Weiss reaction (Kobayashi et al. 2018). The increased ROS can further mediate membrane lipid peroxidation reaction and generate MDA, and the antioxidant enzyme system, such as the activities of antioxidant enzyme SOD is also severely weakened (Tian et al. 2021). To further study the underlying mechanism of GX in alleviating MIRI, the antioxidant activity was investigated. The results revealed that ischaemia/reperfusion significantly increased the levels of SOD and decreased the level of MDA in mice, and these changes were significantly alleviated by GX. In addition, GX could inhibit ROS production in HR-induced H9c2 cells. This evidence indicated that GX could alleviate IR-induced oxidative stress injury during IR/HR.

Imbalances in iron homeostasis have been reported to be involved in MIRI. Myocardial iron overload has been observed both in the post-MI patients received reperfusion therapy (Paterek et al. 2019) and the rats with myocardial ischaemia-reperfusion (Shan et al. 2021). Our results were consistent with these studies. Results from *in vivo* and *in vitro* experiments showed that distinct iron accumulation was been showed in ischaemia-reperfusion induced cardiac tissues and HR-induced

H9c2 cells. However, the iron deposition was significantly alleviated by GX treatment both *in vivo* and *in vitro*.

To further explore the mechanism of GX in reducing iron deposition, some iron metabolism-related proteins were investigated. As a key member of iron metabolism-associated factors, HIF-1α can regulate the transcription of genes involved in iron utilization, such as TFR1, ceruloplasmin, HMOX1 and DMT1; FPN is responsible for ferrous iron efflux from the cell to the peripheral circulation; FTH is responsible for Ferrous iron storage. Some studies demonstrated that activation of HIF-1α expression induced ischaemic tolerance and conferred a cardio-protective effect to diminish cardiac IR injury (Kido et al. 2005; Xie et al. 2015; Deguchi et al. 2020). However, some other studies indicated that the excessive and prolonged activation of HIF-1α can lead to myocyte death and trigger cardiac rupture (Ikeda et al. 2021). Moreover, activation of HIF-1α induced the expression of TFR1, which in turn increased Fe uptake and iron accumulation and exacerbated heart damage during IR of the rat heart, whereas inhibition of HIF-1α attenuated cardiac IR injury (Tang et al. 2008; Lin et al. 2020; Ikeda et al. 2021). Cardiac FPN

regulated cellular iron homeostasis and was important for cardiac function, and the mRNA and protein expression levels of FPN were significantly reduced in rats' hearts under myocardial IR conditions (Lakhal-Littleton et al. 2015; Tian et al. 2021). Furthermore, FTH was downregulated in animal model of MIRI leading to intracellular iron aggregation, oxidative stress and cardiomyocytes death (Omiya et al. 2009). Consistent with previous reports, we found that the expression of HIF1α was upregulated, whereas the expression of FPN and FTH was downregulated both in ischaemia-reperfusion-induced cardiac tissues and HR-induced H9c2 cells. Interestingly, GX pre-treatment was able to antagonize ischaemia-reperfusion and HR-induced upregulation of HIF1α and downregulation of FPN and FTH. From these, we concluded that GX could regulate iron metabolism-associated factors to maintain the intracellular iron homeostasis both *in vivo* and *in vitro*.

Collectively, our study demonstrated that heart suffering ischaemia-reperfusion injury was exposed to iron accumulation and imbalance of oxidative and antioxidant systems, and GX could reduce oxidative stress levels and iron deposition by regulating iron metabolism-associated proteins, contributing to attenuation of MIRI. However, the specific mechanisms remain unclear. The accumulation of excess intracellular iron and redox efficacy of ferrous ions can trap cardiac cells into a vicious cycle of exacerbated ROS-induced impairment, contributing to membrane lipid peroxidation reaction along with MDA generation, which ultimately lead to ferroptosis (Li et al. 2021). Ferroptosis, characterized by iron-dependent accumulation of lipid hydroperoxides, is crucial for the pathogenic mechanism of MIRI, and precisely targeting ferroptosis mechanisms may be a promising therapeutic option to revert myocardial remodelling (Zhao et al. 2021). Therefore, whether ferroptosis participates in the protective effect of GX on MIRI still needs further investigation.

Conclusions

Our research demonstrated that GX maintained iron homeostasis and reduced oxidative stress levels by regulating iron metabolism-associated proteins, eventually contributing to amelioration of MIRI. These findings provide new evidences that GX may act as a potential candidate for the treatment of MIRI.

Author contributions

Fuqiong Zhou: Conceptualization, Investigation, Writing-Original Draft, Data Curation. Zhengguang Zhang: Methodology, Validation, Data Curation, Writing-Original Draft. Meiyuan Wang: Methodology, Formal analysis. Weina Zhu: Methodology, Visualization. Jie Ruan: Software, Formal analysis. Hongyan Long: Resources, Project administration. Yajie Zhang: Investigation, Writing-Review & Editing, Supervision. Ning Gu: Conceptualization, Supervision, Writing-Review & Editing.

Disclosure statement

No potential conflict of interest was reported by the authors.

Funding

ORCID

Yajie Zhang http://orcid.org/0000-0003-2510-6015

Data availability statement

The datasets generated and/or analysed during the current study are not publicly available since they are still under further study, but are available from the corresponding author on reasonable request.

References

Abbaspour N, Hurrell R, Kelishadi R. 2014. Review on iron and its importance for human health. J Res Med Sci. 19:164–174.
Bugger H, Pfeil K. 2020. Mitochondrial ROS in myocardial ischemia reperfusion and remodeling. Biochim Biophys Acta Mol Basis Dis. 1866(7):165768.
Bulluck H, Rosmini S, Abdel-Gadir A, White SK, Bhuva AN, Treibel TA, Fontana M, Ramlall M, Hamarneh A, Sirker A, et al. 2016. Residual myocardial iron following intramyocardial hemorrhage during the convalescent phase of reperfused ST-segment-elevation myocardial infarction and adverse left ventricular remodeling. Circ Cardiovasc Imaging. 9(10):e004940.
Cui Y, Wang Q, Chang R, Aboragah A, Loor JJ, Xu C. 2021. Network pharmacology-based analysis of *Pogostemon cablin* (Blanco) Benth beneficial effects to alleviate nonalcoholic fatty liver disease in mice. Front Pharmacol. 12:789430.
D'Souza E. 2019. An overview and awareness of acute coronary syndrome based on risk factors, early clinical assessment tools, and improving clinical outcomes. J Dr Nurs Pract. 12(1):125–131.
Deguchi H, Ikeda M, Ide T, Tadokoro T, Ikeda S, Okabe K, Ishikita A, Saku K, Matsushima S, Tsutsui H. 2020. Roxadustat markedly reduces myocardial ischemia reperfusion injury in mice. Circ J. 84(6):1028–1033.
Domienik-Karłowicz J, Kupczyńska K, Michalski B, Kapłon-Cieślicka A, Darocha S, Dobrowolski P, Wybraniec M, Wańha W, Jaguszewski M. 2021. Fourth universal definition of myocardial infarction. Selected messages from the European Society of Cardiology document and lessons learned from the new guidelines on ST-segment elevation myocardial infarction and non-ST-segment elevation-acute coronary syndrome. Cardiol J. 28(2):195–201.
Du T, Zhang Z. 2022. Discussion on correlation between autophagy and myocardial ischemia-reperfusion injury from the theory of qi, blood and fluid in Chinese medicine. China J Tradit Chin Med Pharm. 36:7086–7088. Chinese.
Duarte TL, Talbot NP, Drakesmith H. 2021. NRF2 and hypoxia-inducible factors: key players in the redox control of systemic iron homeostasis. Antioxid Redox Signal. 35(6):433–452.
Dunn LL, Kong SMY, Tumanov S, Chen W, Cantley J, Ayer A, Maghzal GJ, Midwinter RG, Chan KH, Ng MKC, et al. 2021. Hmox1 (Heme oxygenase-1) protects against ischemia-mediated injury via stabilization of HIF-1alpha (Hypoxia-inducible factor-1alpha). Arterioscler Thromb Vasc Biol. 41(1):317–330.
Ge H, Lin W, Lou Z, Chen R, Shi H, Zhao Q, Lin Z. 2022. Catalpol alleviates myocardial ischemia reperfusion injury by activating the Nrf2/HO-1 signaling pathway. Microvasc Res. 140:104302.
Hirota K. 2019. An intimate crosstalk between iron homeostasis and oxygen metabolism regulated by the hypoxia-inducible factors (HIFs). Free Radic Biol Med. 133:118–129.
Hirst J. 2013. Mitochondrial complex I. Annu Rev Biochem. 82:551–575.
Huang W, Yang Y, Zeng Z, Su M, Gao Q, Zhu B. 2016. Effect of *Salvia miltiorrhiza* and ligustrazine injection on myocardial ischemia/reperfusion and hypoxia/reoxygenation injury. Mol Med Rep. 14(5):4537–4544.
Ibanez B, Heusch G, Ovize M, Van de Werf F. 2015. Evolving therapies for myocardial ischemia/reperfusion injury. J Am Coll Cardiol. 65(14):1454–1471.
Ikeda M, Ide T, Tadokoro T, Miyamoto HD, Ikeda S, Okabe K, Ishikita A, Sato M, Abe K, Furusawa S, et al. 2021. Excessive hypoxia-inducible factor-1alpha expression induces cardiac rupture via p53-dependent apoptosis after myocardial infarction. J Am Heart Assoc. 10(17):e020895.

Kido M, Du L, Sullivan CC, Li X, Deutsch R, Jamieson SW, Thistlethwaite PA. 2005. Hypoxia-inducible factor 1-alpha reduces infarction and attenuates progression of cardiac dysfunction after myocardial infarction in the mouse. J Am Coll Cardiol. 46(11):2116–2124.

Kobayashi M, Suhara T, Baba Y, Kawasaki NK, Higa JK, Matsui T. 2018. Pathological roles of iron in cardiovascular disease. Curr Drug Targets. 19(9):1068–1076.

Lakhal-Littleton S. 2019. Mechanisms of cardiac iron homeostasis and their importance to heart function. Free Radic Biol Med. 133:234–237.

Lakhal-Littleton S, Wolna M, Carr CA, Miller JJ, Christian HC, Ball V, Santos A, Diaz R, Biggs D, Stillion R, et al. 2015. Cardiac ferroportin regulates cellular iron homeostasis and is important for cardiac function. Proc Natl Acad Sci USA. 112(10):3164–3169.

Li JY, Liu SQ, Yao RQ, Tian YP, Yao YM. 2021. A novel insight into the fate of cardiomyocytes in ischemia-reperfusion injury: from iron metabolism to ferroptosis. Front Cell Dev Biol. 9:799499.

Li T, Tian H, Li J, Zuo A, Chen J, Xu D, Guo Y, Gao H. 2019. Overexpression of lncRNA Gm2691 attenuates apoptosis and inflammatory response after myocardial infarction through PI3K/Akt signaling pathway. IUBMB Life. 71(10):1561–1570.

Liang B, Liang Y, Li R, Zhang H, Gu N. 2021. Integrating systematic pharmacology-based strategy and experimental validation to explore the synergistic pharmacological mechanisms of Guanxin V in treating ventricular remodeling. Bioorg Chem. 115:105187.

Liang B, Qu Y, Zhao QF, Gu N. 2020. Guanxin V for coronary artery disease: a retrospective study. Biomed Pharmacother. 128:110280.

Liang B, Zhang XX, Li R, Gu N. 2022a. Guanxin V protects against ventricular remodeling after acute myocardial infarction through the interaction of TGF-beta1 and Vimentin. Phytomedicine. 95:153866.

Liang B, Zhang XX, Li R, Zhu YC, Tian XJ, Gu N. 2022b. Guanxin V alleviates acute myocardial infarction by restraining oxidative stress damage, apoptosis, and fibrosis through the TGF-beta1 signalling pathway. Phytomedicine. 100(154077):154077.

Lin CF, Hsu KC, HuangFu WC, Lin TE, Huang HL, Pan SL. 2020. Investigating the potential effects of selective histone deacetylase 6 inhibitor ACY1215 on infarct size in rats with cardiac ischemia-reperfusion injury. BMC Pharmacol Toxicol. 21(1):21.

Lok CN, Ponka P. 1999. Identification of a hypoxia response element in the transferrin receptor gene. J Biol Chem. 274(34):24147–24152.

Ma H, Hao J, Liu H, Yin J, Qiang M, Liu M, He S, Zeng D, Liu X, Lian C, et al. 2022. Peoniflorin preconditioning protects against myocardial ischemia/reperfusion injury through inhibiting myocardial apoptosis: risk pathway involved. Appl Biochem Biotechnol. 194(3):1149–1165.

Mahtta D, Sudhakar D, Koneru S, Silva GV, Alam M, Virani SS, Jneid H. 2020. Targeting inflammation after myocardial infarction. Curr Cardiol Rep. 22(10):110.

Mukhopadhyay CK, Mazumder B, Fox PL. 2000. Role of hypoxia-inducible factor-1 in transcriptional activation of ceruloplasmin by iron deficiency. J Biol Chem. 275(28):21048–21054.

Nakamura T, Naguro I, Ichijo H. 2019. Iron homeostasis and iron-regulated ROS in cell death, senescence and human diseases. Biochim Biophys Acta Gen Subj. 1863(9):1398–1409.

Omiya S, Hikoso S, Imanishi Y, Saito A, Yamaguchi O, Takeda T, Mizote I, Oka T, Taneike M, Nakano Y, et al. 2009. Downregulation of ferritin heavy chain increases labile iron pool, oxidative stress and cell death in cardiomyocytes. J Mol Cell Cardiol. 46(1):59–66.

Paterek A, Mackiewicz U, Mączewski M. 2019. Iron and the heart: a paradigm shift from systemic to cardiomyocyte abnormalities. J Cell Physiol. 234(12):21613–21629.

Qian ZM, Wu XM, Fan M, Yang L, Du F, Yung WH, Ke Y. 2011. Divalent metal transporter 1 is a hypoxia-inducible gene. J Cell Physiol. 226(6):1596–1603.

Ramachandra CJA, Hernandez-Resendiz S, Crespo-Avilan GE, Lin YH, Hausenloy DJ. 2020. Mitochondria in acute myocardial infarction and cardioprotection. EBioMedicine. 57:102884.

Ravingerova T, Kindernay L, Bartekova M, Ferko M, Adameova A, Zohdi V, Bernatova I, Ferenczyova K, Lazou A. 2020. The molecular mechanisms of iron metabolism and its role in cardiac dysfunction and cardioprotection. Int J Mol Sci. 21(21):7889.

Romney SJ, Newman BS, Thacker C, Leibold EA. 2011. HIF-1 regulates iron homeostasis in Caenorhabditis elegans by activation and inhibition of genes involved in iron uptake and storage. PLoS Genet. 7(12):e1002394.

Shan X, Lv ZY, Yin MJ, Chen J, Wang J, Wu QN. 2021. The protective effect of cyanidin-3-glucoside on myocardial ischemia-reperfusion injury through ferroptosis. Oxid Med Cell Longev. 2021:8880141.

Song M, Huang L, Zhao G, Song Y. 2013. Beneficial effects of a polysaccharide from Salvia miltiorrhiza on myocardial ischemia-reperfusion injury in rats. Carbohydr Polym. 98(2):1631–1636.

Tang WH, Wu S, Wong TM, Chung SK, Chung SS. 2008. Polyol pathway mediates iron-induced oxidative injury in ischemic-reperfused rat heart. Free Radic Biol Med. 45(5):602–610.

Tian H, Xiong Y, Zhang Y, Leng Y, Tao J, Li L, Qiu Z, Xia Z. 2021. Activation of NRF2/FPN1 pathway attenuates myocardial ischemia-reperfusion injury in diabetic rats by regulating iron homeostasis and ferroptosis. Cell Stress Chaperones. 27(2):149–164.

Vela D. 2020. Keeping heart homeostasis in check through the balance of iron metabolism. Acta Physiol (Oxf). 228(1):e13324.

Wei R, Zhang R, Li H, Li H, Zhang S, Xie Y, Shen L, Chen F. 2018. MiR-29 targets PUMA to suppress oxygen and glucose deprivation/reperfusion (OGD/R)-induced cell death in hippocampal neurons. Curr Neurovasc Res. 15(1):47–54.

Wei Y, Xu M, Ren Y, Lu G, Xu Y, Song Y, Ji H. 2016. The cardioprotection of dihydrotanshinone I against myocardial ischemia-reperfusion injury via inhibition of arachidonic acid omega-hydroxylase. Can J Physiol Pharmacol. 94(12):1267–1275.

Wen J, Wang D, Cheng L, Wu D, Qiu L, Li M, Xie Y, Wu S, Jiang Y, Bai H, et al. 2021. The optimization conditions of establishing an H9c2 cardiomyocyte hypoxia/reoxygenation injury model based on an AnaeroPack System. Cell Biol Int. 45(4):757–765.,.

Wu F, Ye B, Wu X, Lin X, Li Y, Wu Y, Tong L. 2020. Paeoniflorin on rat myocardial ischemia reperfusion injury of protection and mechanism research. Pharmacology. 105(5-6):281–288.

Xiang M, Lu Y, Xin L, Gao J, Shang C, Jiang Z, Lin H, Fang X, Qu Y, Wang Y, et al. 2021. Role of oxidative stress in reperfusion following myocardial ischemia and its treatments. Oxid Med Cell Longev. 2021:6614009.

Xie L, Pi X, Wang Z, He J, Willis MS, Patterson C. 2015. Depletion of PHD3 protects heart from ischemia/reperfusion injury by inhibiting cardiomyocyte apoptosis. J Mol Cell Cardiol. 80:156–165.

Yang W, Lai Q, Zhang L, Zhang Y, Zhang Y, Yu B, Li F, Kou J. 2021. Mechanisms dissection of the combination GRS derived from ShengMai preparations for the treatment of myocardial ischemia/reperfusion injury. J Ethnopharmacol. 264:113381.

Yong C, Zhang Z, Huang G, Yang Y, Zhu Y, Qian L, Tian F, Liu L, Wu Q, Xu Z, et al. 2021. Exploring the critical components and therapeutic mechanisms of Perilla frutescens L. in the treatment of chronic kidney disease via network pharmacology. Front Pharmacol. 12:717744.

Zeng H, Wang L, Zhang J, Pan T, Yu Y, Lu J, Zhou P, Yang H, Li P. 2021. Activated PKB/GSK-3beta synergizes with PKC-delta signaling in attenuating myocardial ischemia/reperfusion injury via potentiation of NRF2 activity: therapeutic efficacy of dihydrotanshinone-I. Acta Pharm Sin B. 11(1):71–88.

Zhang Q, Shi J, Guo D, Wang Q, Yang X, Lu W, Sun X, He H, Li N, Wang Y, et al. 2020. Qishen Granule alleviates endoplasmic reticulum stress-induced myocardial apoptosis through IRE-1-CRYAB pathway in myocardial ischemia. J Ethnopharmacol. 252:112573.

Zhang X, Shao C, Cheng S, Zhu Y, Liang B, Gu N. 2021. Effect of Guanxin V in animal model of acute myocardial infarction. BMC Complement Med Ther. 21(1):72.

Zhang Z, Yan J, Chang Y, ShiDu Yan S, Shi H. 2011. Hypoxia inducible factor-1 as a target for neurodegenerative diseases. Curr Med Chem. 18(28):4335–4343.

Zhao WK, Zhou Y, Xu TT, Wu Q. 2021. Ferroptosis: opportunities and challenges in myocardial ischemia-reperfusion injury. Oxid Med Cell Longev. 2021:9929687.

Zuo K, Ke F, Gu N. 2015. Effect and mechanism of Guanxin V mixture on ventricular remodeling after acute myocardial infarction. Chin J Exp Tradit Med Form. 21:147–150. Chinese.